

# Direct measurement of lateral transport in membranes by using time-resolved spatial photometry

(digital video image analysis/fluorescence recovery after photobleaching/low-light-level microscopy)

H. G. KAPITZA\*, G. MCGREGOR†, AND K. A. JACOBSON

Department of Anatomy and Cancer Research Center, Laboratories for Cell Biology, 108 Swing Building 217H, University of North Carolina at Chapel Hill, Chapel Hill, NC 27514

Communicated by Gregorio Weber, March 4, 1985

**ABSTRACT** Spatially resolving light detectors allow, with proper calibration, quantitative analysis of the variations in two-dimensional intensity distributions over time. An ultrasensitive microfluorometer was assembled by using as a detector a microchannel plate-intensified video camera. The camera was interfaced with a software-based digital video analysis system to digitize, average, and process images and to directly control the timing of the experiments to minimize exposure of the specimen to light. The detector system has been characterized to allow its use as a photometer. A major application has been to perform fluorescence recovery after photobleaching measurements by using the camera in place of a photomultiplier tube (video-FRAP) with the goal of detecting possible anisotropic diffusion or convective flow. Analysis of the data on macromolecular diffusion in homogenous aqueous glycol solutions yielded diffusion constants in agreement with previous measurements. Results on lipid probe diffusion in dimyristoylphosphatidylcholine multibilayers indicated that at temperatures above the gel-to-liquid crystalline phase transition diffusion is isotropic, and analysis of video-FRAP data yielded diffusion coefficients consistent with those measured previously by using spot photobleaching. However, lipid probes in these multibilayers held just below the main phase transition temperature exhibited markedly anisotropic diffusive fluxes when the bleaching beam was positioned proximate to domain boundaries in the  $P\beta'$  phase. Lipid probes and lectin receptor complexes diffused isotropically in fibroblast surface membranes with little evidence for diffusion channeled parallel to stress fibers. A second application was to trace the time evolution of cell surface reactions such as patching. The feasibility of following, on the optical scale, the growth of individual receptor clusters induced by the ligand wheat germ agglutinin was demonstrated.

During the past 20 years application of low-light-level image intensification to biological microscopy has seen continuous development (1-5). Several recent studies have indicated the usefulness of these techniques for quantitative microfluorescence studies (6-12; R. Walters and M. Berns, personal communication), and, in this study, we have employed a camera consisting of a microchannel-plate (MCP) image intensifier (high, nearly linear gain; high resolution; low noise; low geometric distortion) coupled to a video detector. This ultrasensitive spatial detector was combined with a small digitizing, data-storing, and analyzing microcomputer to allow investigation of the redistribution of fluorescent probes within cell membranes and the cytoplasm using minimal excitation energy and low-fluorophore surface density. Since intensity measurements with such detectors provide both temporal and spatial resolution, the method has been named time-resolved spatial photometry (TRSP). The experiments

described below combined this approach with the fluorescence recovery after photobleaching (FRAP) method (ref. 13; for review, see ref. 14) to investigate details of lateral transport phenomena in membranes.

## MATERIALS AND METHODS

**Instrumentation.** The optical setup used for TRSP and video FRAP is shown in Fig. 1 and is based on a conventional spot photobleaching setup (15). The low-light-level detector and image digitizing computer replaces the photomultiplier tube, amplifiers, and readout. To test the linearity and spatial distortion of our low-light-level television (L3TV)-camera detector (Intensicon 8; Lenzar, Riviera Beach, FL), an appropriate set of optical bench tests was performed and will be described elsewhere (unpublished data). These tests allowed selection of that region on the camera faceplate giving rise to the least geometric distortion and greatest uniformity in intensity response. A  $100 \times 100$  pixel area was defined, inside the full  $320 \times 256$  pixel image array, covering the specified scan area on the photocathode. Overall camera gain was monitored by output voltages proportional to the microchannel plate bias voltage and the vidicon gain. These voltages remained constant during examination of a given scene when fluorescence fading was minimized. Digitizing and processing of the video data were performed by using dedicated circuit boards (QVG/DAF 120; Datacube, Peabody, MA), which also provide "look-up tables" for control of gray level mapping (e.g., red-green-blue color display using software-controlled pseudocolors). These boards reside together with an LSI 11/23 microcomputer (Digital Equipment, Maynard, MA) in a box providing a Q-bus backplane, power supply, and data mass storage devices (10-megabyte hard disk, megabyte floppy disk; Disk System 11X, Scientific Micro Systems, Mountain View, CA). Data acquisition was done by averaging several incoming TV frames, as stated in the captions, to produce a single picture with sufficient signal/noise ratio (16). One of every eight incoming frames could be transferred to the host computer for incorporation into the average. (Currently available "on board" arithmetic logic units allow every incoming digitized frame to be counted in the average.) To record images, the fluorescence was excited with the standard Leitz mercury lamp (HBO

Abbreviations: FRAP, fluorescence recovery after photobleaching; TRSP, time-resolved spatial photometry; MCP, microchannel plate; NCAR, National Center for Atmospheric Research; Myr<sub>2</sub>-PtdCho, dimyristoylphosphatidylcholine; egg PtdCho, egg phosphatidylcholine; diI-C<sub>16</sub>(3), 3,3'-dihexadecylindodicarbocyanine iodide; NBD-egg PtdEtn, *N*-4-nitrobenzo-2-oxa-1,3-diazole egg phosphatidylethanolamine; EBTr cells, embryonal bovine trachea cells; Suc-Con A, succinyl-concanavalin A; WGA, wheat germ agglutinin; MBL, multibilayer; AGC, automatic gain control; L3TV, low-light-level television.

\*Present address: Carl Zeiss Company, Oberkochen, Federal Republic of Germany.

†Present address: Amtote Corporation, Hunt Valley, MD 21136.

The publication costs of this article were defrayed in part by page charge payment. This article must therefore be hereby marked "advertisement" in accordance with 18 U.S.C. §1734 solely to indicate this fact.

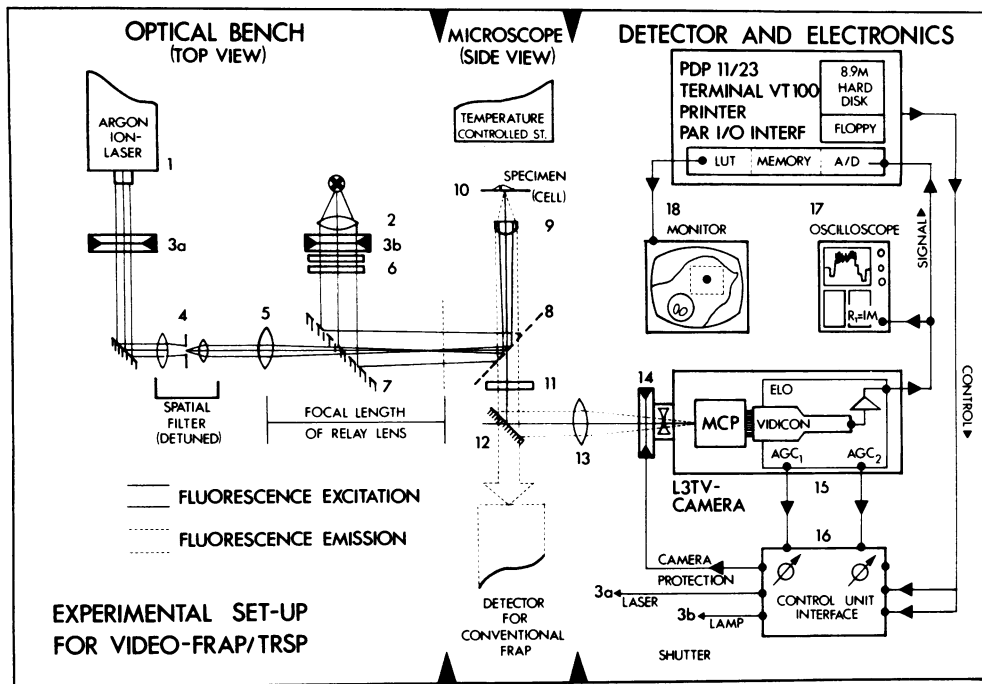


FIG. 1. Setup for TRSP and video-FRAP experiments. Components: 1, argon ion-laser; 2, high-pressure mercury lamp; 3 a and b, electromagnetic shutter; 4, pinhole defining bleached area; 5, relay lens; 6, excitation filters; 7, beam-splitter mirror; 8, dichroic mirror; 9, objective lens; 10, specimen (cell); 11, emission filters; 12, removable surface mirror; 13, eyepiece; 14, camera protection shutter; 15, L3TV camera; 16, control unit; 17, oscilloscope; 18, TV monitor; AGC, automatic gain control; ELO, camera circuitry; LUT, look-up table; PAR I/O, parallel input/output interface.

100W/2) equipped with a heat filter, scatter disc, two high-quality interference filters, and dichroic mirror in series for epi-fluorescence excitation. To create a bleached region in the image for video-FRAP, a circular spot of nearly constant intensity along its radius was formed by slightly overfilling the pinhole of a detuned spatial filter (17) with an argon ion laser beam (model 164, Spectra Physics, Mountain View, CA) and focusing this modified beam on the intermediate image plane of the microscope.

A typical video-FRAP analysis was performed in the following sequence. First, an averaged image prebleach image was acquired and stored by the computer. Next, a bleach pulse, generated by a laser beam modified as described above, created circularly symmetric initial distribution of bleached fluorophores. Immediately after bleaching, an averaged image of this distribution was acquired and stored. At preset intervals after this image, four subsequent averaged images were acquired and stored to record the information about the fluorescence redistribution after photobleaching. Images were digitized after a 1-sec exposure to allow the camera to fully adjust to ambient emission from the specimen. The intensity of features far from the bleached region remained constant, indicating the generalized photobleaching of the specimen was negligible during the time course of these experiments.

**Data Output and Analysis.** Prior to image analysis, the averaged images were averaged in space (smoothing) by sliding a  $3 \times 3$  kernel along each row of pixels and replacing the center pixel with the average of all nine pixels of the kernel (16). Next, the five postbleach patterns were each subtracted from the first (prebleach pattern), giving five images showing only the changes relative to the prebleach condition. All constant intensities including system background noise were removed by this step. Data were viewed in pseudo colors for preliminary analysis and by isointensity contour maps for final presentation (see below). These maps were generated on a VAX 11/780 using the National Center for Atmospheric Research (NCAR) graphics programs.

As discussed below, the video-FRAP data indicated small or negligible departures from isotropic diffusion. On this basis, a simple analysis could be adopted based on an infinite plane medium. The initial condition is given by a square well in the concentration of unbleached fluorophores of radius  $r$

$= a$ , the radius of the focused laser beam in the specimen plane as measured from the optical axis ( $r = 0$ ). Because all subsequent frames are subtracted from the initial prebleach frame, in effect, the decay of the concentration of the bleached fluorophores in time,  $t$ , is observed. The decay of this concentration on the optical axis [ $C(r = 0, t)$ ] can be described by a diffusing fraction that decays exponentially (ref. 18; equation 3.11) and a nondiffusing fraction represented by a parameter,  $B$ :

$$C(0, t) = C_0[1 - \exp(-a^2/4Dt)] + B, \quad [1]$$

where  $D$  is the diffusion coefficient of the mobile species and  $C_0$  represents the concentration of the diffusible, bleached fluorophore on the optical axis at time zero (immediately after photobleaching). Using a microcomputer, Eq. 1 was linearized on a semilogarithmic plot and  $B$  was adjusted to give the optimal fit according to a linear regression analysis; the diffusion coefficient was extracted from the slope of the curve.

**Reagents and Sample Preparation. Aqueous solutions.** Bovine serum albumin (Sigma) was labeled with fluorescein isothiocyanate, dialyzed against phosphate-buffered saline (P<sub>i</sub>/NaCl), mixed at 37°C with 90% glycerol, and allowed to equilibrate overnight at 37°C prior to the preparation of the final specimen. Ten microliters of the mixture was squeezed firmly between cleaned slide and coverslip, resulting in a fluid layer typically  $5 \pm 2 \mu\text{m}$  thick. The excess fluid was removed and the specimen was sealed with paraffin. The resulting fluorescence intensity was dim to the eye but easily detected by the camera.

**Lipid multibilayers (MBLs).** Lipid MBLs were prepared as described (19) from dimyristoylphosphatidylcholine (Myr<sub>2</sub>-PtdCho) and purified egg phosphatidylcholine (egg PtdCho), both obtained from Sigma. They were doped with low concentrations (<0.1%) of the fluorescent lipid analog 3,3'-dihexadecylindodicarbocyanine iodide [diI-C<sub>16</sub>(3)], a generous gift of A. Waggoner, or *N*-4-nitrobenzo-2-oxa-1,3-diazole egg phosphatidylethanolamine (NBD-egg PtdEtn; Avanti Polar Lipids).

**Cells.** Human neonatal foreskin diploid fibroblasts, strain BG 9, and embryonal bovine trachea cells (EBTr cells) were

cultured on coverslips labeled with the lipid probe diI-C<sub>16</sub>(3) as described (23). Fluoresceinated or rhodamine-conjugated succinyl-concanavalin A (Suc-Con A) and wheat germ agglutinin (WGA) were obtained from E-Y Laboratories, San Mateo, CA. These lectins were incubated with cells at concen-

trations of 20–50  $\mu\text{g/ml}$  in P<sub>i</sub>/NaCl containing Ca<sup>2+</sup> and Mg<sup>2+</sup> for 10–15 min at room temperature in the dark, followed by repeated washing with the P<sub>i</sub>/NaCl. The microscope studies were carried out at room temperature within the first 90 min after labeling.

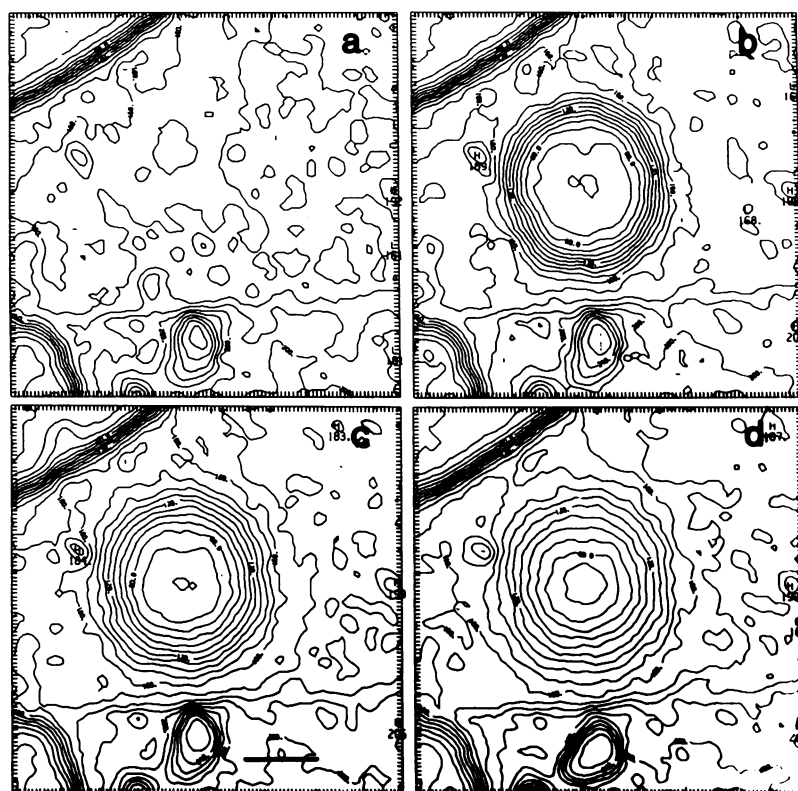
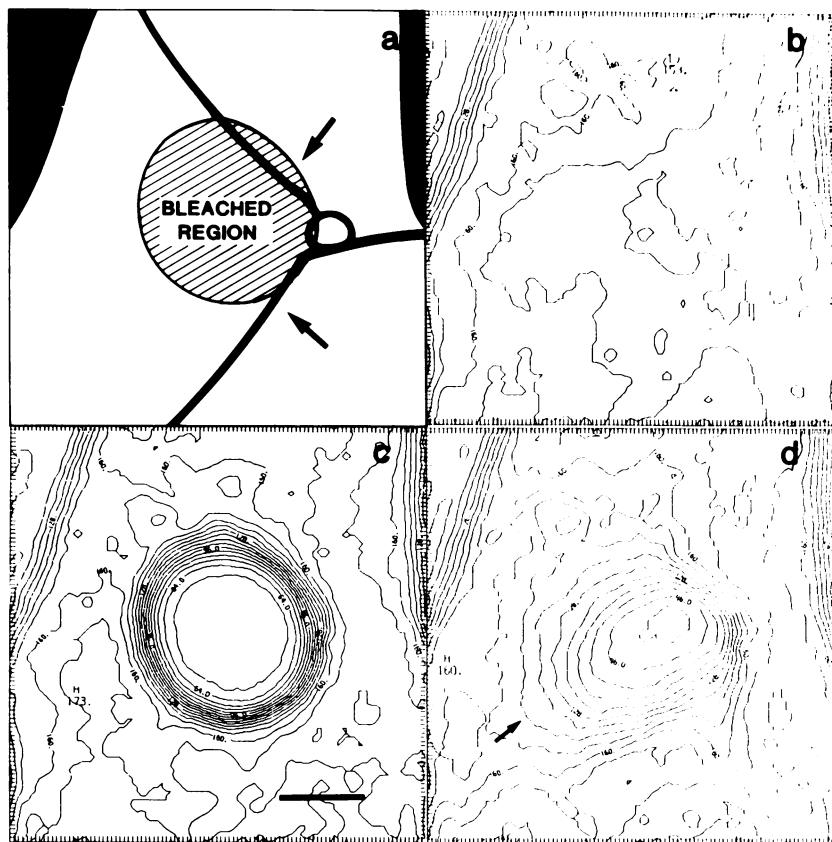


FIG. 2. (Upper) Video-FRAP data for diI-C<sub>16</sub>(3) diffusion in Myr<sub>2</sub>-PtdCho MBLs just below the transition temperature (23.5°C). (a) Schematic of MBL structure showing how an  $\approx 10\text{-}\mu\text{m}$  (diameter) laser bleaching beam was positioned near the aqueous boundaries (arrows) to create an anisotropic recovery condition. White areas represent MBL regions; shaded area is the bleached regions and the black areas and lines represent aqueous zones and boundaries, respectively. Drawing was made from video image of specimen. (b–d) NCAR isointensity contour plots taken before the bleach (b), immediately after bleach (c), and 900 sec after bleach (d). Bleach time, 1 sec. Each plot was constructed from the average of 32 frames that was smoothed. Bar in c is 5  $\mu\text{m}$  ( $\times 25$  objective). Each tick mark represents the length of 1 pixel. (Lower) Video-FRAP data for diI-C<sub>16</sub>(3) diffusion in the plasma membrane of BG 9 cells displayed with the NCAR isointensity plots taken (clockwise from the left corner) prior to bleach, immediately after bleach, 10 sec after bleach, and 30 sec after bleach. Bleach time, 2 sec; bleaching beam diameter, 9.2  $\mu\text{m}$ . Each plot was constructed from the average of 8 frames that was smoothed. The temperature was about 0°C to slow diffusion and the diffusion coefficient calculated from the differenced images was  $1 \times 10^{-9} \text{ cm}^2/\text{sec}$ . Bar in c is 5  $\mu\text{m}$ .

## RESULTS AND DISCUSSION

**The Camera as a Photometric Detector.** The intensity response of the detector-computer system over three decades beginning at an apparent signal/noise ratio of 1 was shown to be approximately linear (data not shown). Black level was "fixed" by positioning a black tape mask very close to the intensifier face plate and obscuring <15% of the field of view. Nonuniformity in the spatial detector intensity response (shading) was measured to be within  $\pm 3\%$  and the geometric distortion, in the part of the detector area used for experiments, was negligible. Analog and digital readouts of linear intensity scans across a uniformly fluorescent specimen indicated that the detector did not exhibit any systematic shading with circular symmetry ("hay-stack response"). The time-response of the system to intrascenic intensity changes was much faster (<1 sec) than necessary for these experiments, as judged by rapidly changing the illumination intensity of a fixed pattern. The lateral spatial resolution of the microscope-camera-computer system was judged to be considerably better than that required for these experiments by observing the output intensity scans generated from both a stage micrometer and small bright (<1  $\mu\text{m}$ ) fluorescent particles. The latter test also allowed definition of the voltage acceptance "window" of the digitizer (A/D converter) to avoid clipping of high-intensity features. The stage micrometer also provided a direct method for calibrating distances in a specimen.

**Measurement of Lateral Transport by Photobleaching and TRSP (Video-FRAP).** The advantage of using a detector with

spatial resolution as opposed to a photomultiplier lies in the ability to discern both anisotropic diffusion and flow-type recoveries after photobleaching. First, the accuracy of diffusion coefficients ( $D$ ) derived from the video-FRAP data (see Eq. 1, above) was established for isotropic and homogeneous samples, both in the absolute values of  $D$  and in their temperature dependences (data not shown). Membrane lateral diffusion was checked by using the lipid analog NBD-PtdEtn in egg PtdCho MBLs and the values were in reasonable agreement with previous measurements (20). Similarly, the translational diffusion coefficients for fluorescein-bovine serum albumin and rhodamine Suc-Con A in 90% glycerol/P<sub>i</sub>/NaCl mixtures agreed with previous measurements and the prediction of the Stokes-Einstein equation (21).

Additional studies using dil-C<sub>16</sub>(3)-labeled Myr<sub>2</sub>-PtdCho MBLs just below the transition temperature demonstrated the ability of the video-FRAP system to report anisotropic transport events (Fig. 2 *Upper*). MBLs can be considered as an array of closely spaced and squashed large multilamellar liposomes separated by aqueous boundaries (19). When a region proximate to such an aqueous boundary is bleached, as shown schematically in Fig. 2 *Upper a*, we expect an anisotropic recovery because diffusional transport across the boundary will be extremely slow. Indeed, the maximal influx of unbleached fluorophores occurs from that part of the liposome opposite the boundary, as seen by the much more rapid erosion of the edge of the bleached area in this region (arrow in Fig. 2 *Upper d*). The macroscopic two-dimensional diffusion coefficient is presumably isotropic, in this case,

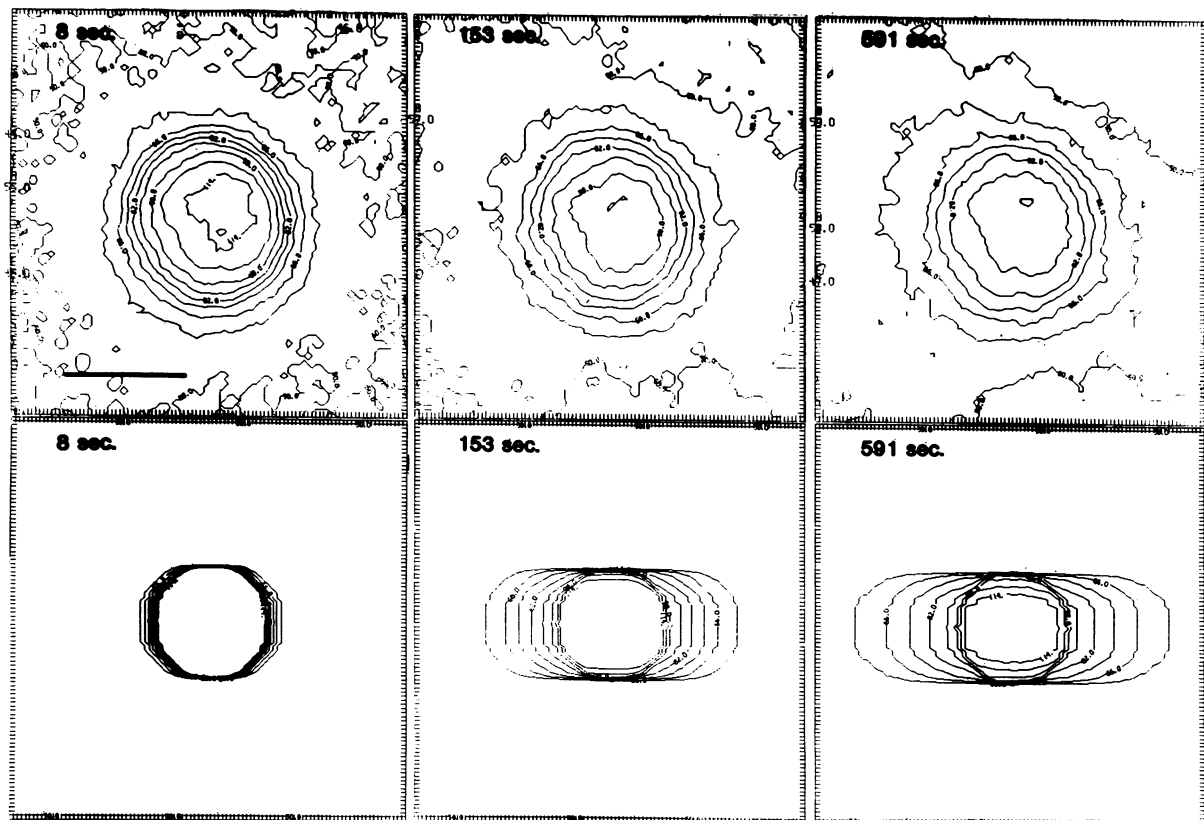


FIG. 3. (*Upper*) Differenced video-FRAP data for TMR-WGA-receptor diffusion on EBTr cells displayed with NCAR isointensity contour plots taken 8, 153, and 591 sec after bleach. Each plot was constructed from the average of 32 frames that was smoothed. Bleach beam diameter, 5.6  $\mu\text{m}$ ; bleach time, 3 sec;  $\times 40/1.3$  oil objective used; diffusion coefficient calculated according to isotropic analysis,  $2.3 \pm 0.4 \times 10^{-10}$   $\text{cm}^2/\text{sec}$ ; mobile fraction, 39%. Bar is 5  $\mu\text{m}$ . The uncertainty in the contour position was assessed by estimating the noise ( $\Delta I$ ) in pixel values in regions of constant intensity from line readout program outputs. The uncertainty in position is related to the local slope ( $m$ ) of the bleached profile through  $\Delta r = \Delta I/m$ . In regions where the slope changes rapidly,  $\Delta r \leq \pm$  pixel length (tick mark); in regions where the intensity is slowly changing,  $\Delta r \approx \pm 4$  pixel lengths (tick marks). (*Lower*) Channeled diffusion model imaged digitally based on only allowing diffusion to occur parallel to the  $x$  axis in 0.2- $\mu\text{m}$  strips. Recovery after same times as in *Upper*. Model based on linear diffusion starting from an extended source of limited extent (equation 2.15, ref. 18).

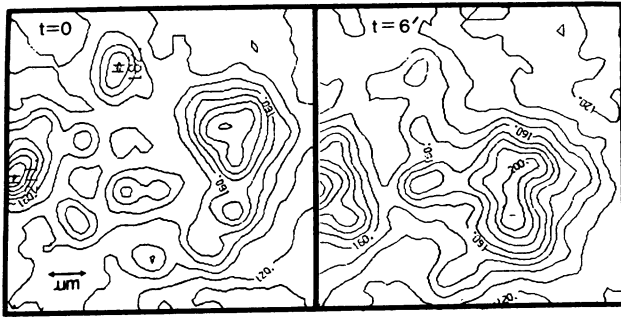


FIG. 4. Use of nonphotobleaching TRSP to monitor details of patching reaction when receptor WGA is added to BG 9 human fibroblasts. At times 0 and 6 min, 8 frames were averaged. Smoothing was performed prior to constructing the isointensity contour map. A  $\times 40/1.3$  oil objective was employed. A micron mark is indicated in the lower left of the left panel.

but the position of the bleaching beam with respect to sample structures rendered the fluorescence recovery highly anisotropic. Other experiments revealed examples of channeled diffusion along linear defects in the MBLs (22).

Measurements of lipid probe diI-C<sub>16</sub>(3) diffusion as a function of temperature were made on spread fibroblasts in monolayer culture (Fig. 2 Lower) and were consistent with earlier data for which the spot photobleaching method was used (23). No significant departures from circular isointensity contour lines were observed, implying that the diffusion process was isotropic. No correlation between the fluorescence recovery pattern and the underlying fiber bundle orientation was apparent. Recovery for the lipid probes was nearly complete in all cases examined.

Typical results for the lateral diffusion of WGA or Suc-Con A receptor complexes in the fibroblast plasma membrane are given in Fig. 3 Upper. The recovery appears to proceed isotropically within the limits imposed by noise with  $D$  values in the range of  $10^{-11}$  to  $5 \times 10^{-10}$  cm<sup>2</sup>/sec and mobile fractions ranging from 20% to 60%, consistent with earlier data (15, 24). No pronounced anisotropy was observed despite the fact that regions over dense arrays of stress fibers (visualized by phase contrast) were selected for measurement. Smith *et al.* (25) suggested that lateral diffusion of some receptors could be channeled by the stress fibers. We have modeled the extreme case of this situation where diffusion is only permitted in channels parallel to the  $x$  axis, loaded the calculated values into the image memory, and then plotted isointensity contour maps; the results are seen in Fig. 3 Lower. We have not observed actual maps of this form; occasionally, anisotropic recoveries appeared but these appeared to reflect a nonuniform bleach. Occasionally, Suc-Con A receptor complexes found directly over fiber bundles appeared to be immobilized, presumably because this lectin can bind to the extracellular fibronectin arrays (26) that are often aligned with internal stress fibers (27).

**Redistribution of Cell Surface Molecules Followed by TRSP.** Redistribution of cell surface molecules and molecules and organelles within the cytoplasm can be followed quantitatively without photobleaching by using TRSP. In Fig. 4, the details of patching of WGA receptors upon the addition of WGA are seen in isointensity contour maps from images taken 6 min apart. Examination of these maps revealed increased intensity within progressively contracting patches. These studies indicate that quantitative kinetic details of cell surface and cytoplasmic reactions can now be examined with much greater ease and efficiency than that

afforded by low-light photography and subsequent densitometry.

We gratefully acknowledge the technical assistance of Mr. Bruce Holifield and Ms. Donna O'Dell. The advice and cooperation of Messrs. Brad Ganther, Robert Jones, and Mark James, President, Chief Engineer, and Project Engineer, respectively, of Lenzar Optics, Riviera Beach, FL, and of Mr. Stan Karadanis, President of Datacube, Peabody, MA, greatly facilitated progress on this project. We acknowledge the generous assistance of Dr. Richard Johnson, Chairman of the Curriculum in Biomedical Engineering and Mathematics, as well as Gerald Robinson, Ben Aycock, and the staff of the A. F. Fortune Biomedical Computing Center at the University of North Carolina at Chapel Hill. We also express special thanks to Dr. C. R. Hackenbrock, Chairman, Department of Anatomy, for his support and encouragement throughout the course of this project. This project was supported by grants from the American Cancer Society (CD-181), the American Heart Association (Grant-in-Aid 83-1385), the National Institutes of Health (GM-29234), and the Deutsche Forschungsgemeinschaft (DFG Ka 617-1) of West Germany.

1. Reynolds, G. T. (1964) *IEEE Trans. Nucl. Sci.* NS11(3), 147-151.
2. Kohen, E., Thorell, B., Kohen, C. & Salmon, J. (1974) *Adv. Biol. Med. Phys.* 15, 271-295.
3. Rose, B. & Lowenstein, W. (1975) *Science* 190, 1204-1206.
4. Willingham, M. C. & Pastan, I. (1978) *Cell* 13, 501-505.
5. Reynolds, G. T. & Taylor, D. L. (1980) *Bioscience* 30, 586-592.
6. Oliver, J. & Berlin, R. D. (1982) *Philos. Trans. R. Soc. London Ser. B* 299, 215-235.
7. Agard, D. & Sedat, J. W. (1983) *Nature (London)* 302, 676-681.
8. Tanasurgharn, L., McNeil, P., Reynolds, G. T. & Taylor, D. L. (1984) *J. Cell Biol.* 98, 717-724.
9. Gross, D. & Webb, W. W. (1984) *Biophys. J.* 45, 269 (abstr.).
10. Salmon, E. D., Saxton, W. M., Leslie, R. J., Karow, M. L. & McIntosh, J. R. (1984) *J. Cell Biol.* 99, 2157-2164.
11. Boggan, J. E., Walter, R., Edwards, M., Borcich, J. K., Davis, R. L., Koonce, M. & Berns, M. W. (1984) *J. Neurosurg.* 61, 1113-1119.
12. Benson, D., Bryan, J., Plante, A., Gotto, A. M., Jr., & Smith, L. (1984) *J. Cell Biol.* 100, 1309-1323.
13. Peters, R., Peters, J., Tews, K. H. & Baehr, W. (1974) *Biochim. Biophys. Acta* 367, 282-294.
14. Kapitza, H. G. & Jacobson, K. A. (1984) in *Techniques for the Analysis of Membrane Proteins*, eds. Ragan, I. & Cherry, R. J. (Chapman & Hall, London), in press.
15. Jacobson, K. A., Derzko, Z., Wu, E. S., Hou, Y. & Poste, G. (1977) *J. Supramol. Struct.* 5, 565-576.
16. Castleman, K. V. (1979) *Digital Image Processing* (Prentice-Hall, Englewood Cliffs, NJ).
17. Kapitza, H.-G. & Sackmann, E. (1980) *Biochim. Biophys. Acta* 595, 56-64.
18. Crank, J. (1975) *The Mathematics of Diffusion* (Clarendon Press, Oxford).
19. Wu, E. S., Jacobson, K. A. & Papahadjopoulos, D. (1977) *Biochemistry* 16, 3936-3941.
20. Vaz, W. L. C., Derzko, Z. & Jacobson, K. A. (1982) *Cell Surf. Rev.* 8, 84-128.
21. Jacobson, K. A., Wu, E. S. & Poste, G. (1976) *Biochim. Biophys. Acta* 433, 215-222.
22. Kapitza, H.-G., McGregor, G. & Jacobson, K. A. (1984) *Biophys. J.* 45, 89 (abstr.).
23. Jacobson, K. A., Hou, Y., Derzko, Z., Wojcieszyn, J. & Organisciak, D. (1981) *Biochemistry* 20, 5268-5275.
24. Schlessinger, J., Koppel, D. E., Axelrod, D., Jacobson, K., Webb, W. W. & Elson, E. L. (1976) *Proc. Natl. Acad. Sci. USA* 73, 2409-2413.
25. Smith, B. A., Clark, W. R. & McConnell, H. M. (1979) *Proc. Natl. Acad. Sci. USA* 76, 5641-5644.
26. Burrige, K. (1976) *Proc. Natl. Acad. Sci. USA* 73, 4457-4461.
27. Hynes, R. O. & Yamada, K. M. (1982) *J. Cell Biol.* 95, 369-377.